We are IntechOpen,
the world's leading publisher of
Open Access books
Built by scientists, for scientists

6,900
Open access books available

186,000
International authors and editors

200M
Downloads

Our authors are among the

154
Countries delivered to

TOP 1%
most cited scientists

12.2%
Contributors from top 500 universities

CLARIVATE ANALYTICS
BOOK CITATION INDEX
INDEXED

WEB OF SCIENCE™

Selection of our books indexed in the Book Citation Index
in Web of Science™ Core Collection (BKCI)

Interested in publishing with us?
Contact book.department@intechopen.com

Numbers displayed above are based on latest data collected.
For more information visit www.intechopen.com

Femtosecond Laser Lithography in Organic and Non-Organic Materials

Florin Jipa, Marian Zamfirescu, Alin Velea,
Mihai Popescu and Razvan Dabu

Additional information is available at the end of the chapter

http://dx.doi.org/10.5772/56579

1. Introduction

The lithography is a well established technology for fabrication of microelectronic components, integrated optics, microfluidic devices and Micro-Electro-Mechanical-Systems (MEMS) [1,2]. Using energy sources like ultra-violet (UV) photons or X-ray, various patterns are transferred from photo lithographic masks to photoresist materials. Developed for MEMS fabrications, the photoresists are light-sensitive materials. During exposure, chemical reactions are initiated in the irradiated volume, changing the chemical properties of the material. An imprinted pattern can be obtained when the exposed or unexposed material is removed by chemical solvents.

The size of the structures created through lithographic methods depends on the radiation wavelength. The optical diffraction limit represents the limiting factor for obtaining the minimum feature size. As a result, in the UV lithography the exposure wavelength was reduced initially from g-line (436 nm) to h-line (405 nm) and then to i-line (365 nm).

When smaller structures were required for the metal–oxide–semiconductor (MOS) circuits improvement, the UV lamps were replaced with excimer lasers. Deep UV lithography (DUV), based on 248 nm (KrF) and 194 nm (ArF) wavelengths [3,4], is used in semiconductor industry to produce transistors with 90 nm gate lengths. A further decrease of the radiation source to 157 nm wavelength (molecular fluorine) [5] was limited by the low transmission of fused silica material in this spectral range.

High quality crystalline calcium fluoride with low birefringence was grown for mask substrate and refractive lenses fabrication. Some technical difficulties, related to the mask protection,

the requirement of special vacuum chambers and the growth of calcium fluoride material [6,7], have limited the implementation of this technology on large scale.

The 194 nm technology was reconsidered when a new technology, based on a liquid immersion between the last optical components and the photoresist material, was proposed [8]. In this case, the achieved resolution becomes similar to the 157 nm technology in air.

Despite some difficulties, like impurities from liquid immersion or bubbles formation [9,10], the immersion technology was used to manufacture 45 nm features in mass production. Using high-index fluids, it was tested for a 32 nm feature target too [11].

Other nano-technologies, like X-ray lithography [12] and ion/electron beam lithography [13,14], are used to obtain smaller feature size. Using exposure wavelengths under 100 nm, structures smaller than 30 nm were obtained [15]. The high cost of the mask fabrication for X-ray lithography limits the implementation of this technology on large scale production.

Another challenging technique, extreme ultraviolet lithography (EUV), uses a very short wavelength, 13.5 nm, to induce feature size down to 11 nm in photoresist materials [16]. The implementation of this technology is limited due to the complexity of installations for EUV radiation generation and photoresist characteristics like sensitivity and resolution.

Alternative methods like electron/ion beam lithography are used to produce nanometric structures in photoresist materials. A focused electron beam can generate chemical reactions in photoresist materials. This method does not require a photomask to create a pattern. The beam is focused directly in the photoresist material where structures with dimensions less than 30 nm can be obtained [17]. The implementation of this technology as mass volume production is limited by the high price of installations and the long exposure time for large area.

Alternative techniques like nano-imprint (soft) lithography can be used for low-cost pattern imprint. By this method, to create a pattern replica, a stamp or mold is pressed on a photoresist or thermoplastic material. The resulting mold replica can be used to multiply the original mold without complex and high cost production installations. Structures with dimensions under 100 nm were regularly imprinted, becoming the preferred method for high number microdevices fabrication.

All these lithographic methods which use masks or expose directly the photoresist material are limited to bi-dimensional structures. In some applications, such as photonic devices or microfluidics, three-dimensional (3D) structures with high-aspect ratio are needed. In order to create 3D structures, other exposure techniques, like laser holography or laser lithography with near infrared (NIR) femtosecond lasers, are required.

In case of holographic methods, based on the interference of several laser beams, the pattern is directly reconstructed in the photoresist volume. Using the holographic method [18,19], several research groups have obtained periodical structures with sub micrometer features on large surfaces. Nevertheless, the holographic method has some limitations when the design of the structure imposes localized defects in a complex 3D structure.

To overcome this drawback, infrared (IR) femtosecond laser installations with high repetition rate can be used to create 3D structures in photoresist materials. Due to the transparency in

the NIR spectral band, the femtosecond laser pulses can be focused deeply in the photoresist volume. The high NIR photons density created in the focused spot induce two-photons or multi-photons absorption. Chemical reactions are initiated and structural modifications take place similar to the case of a single UV photon absorption.

In this paper we present an IR femtosecond laser processing method which can be used in organic and non-organic photoresist materials lithography. Section 2 is dedicated to micro-structures created by two-photon polymerization (TPP) in organic materials irradiated with femtosecond lasers. The TPP principle, the experimental set-up and processing procedure, as well as some applications of photoresist microstructures, are presented in this section. The non-organic photoresist materials and the main effects related to their interaction with the laser radiation are described in Section 3. Optical micro-lenses and photonic crystals, manufactured by photoresist laser lithography, are presented too. Conclusions are presented in Section 4.

2. Femtosecond laser lithography in organic photoresists

2.1. Principle of photo-polymerization mechanism in organic photoresist materials

Organic photoresist materials are composed by two main molecular components: monomers/oligomers (M) and photo-initiators (I). The monomers are unsaturated molecules and represent 90% from the photoresist material composition. These molecules can be bound in polymeric chains using the energy from a radiation source like photons. Two different photo-mechanisms, Chain Polymerizations and Step Polymerization (Photo-crosslinking), can be used to initiate this conversion.

When the light is used as an exposure energy source, the commonly encountered polymerization mechanism is based on chain propagation. Three stages: initiation, propagation and termination, are involved in this mechanism. The initiation stage starts when the excited photo-initiators (I*), produced in the presence of light, generate active species [20-22] like free radicals (R*), (Equation 1). Afterwards, these radicals interact with monomers, creating a new molecule which has an active termination (Equation 2). Once the process is started, a new monomer is added through this termination to the molecule (Equation 3). In this way, the polymeric chains grow rapidly without any supplementary photons excitations.

During propagation stage (Equation 4), the polymeric chains increase in length, until the active termination encounter a free radical (Equation 5) or an other active termination from a second polymeric chain (Equation 6). Through this coupling effect the formation of the polymeric chain comes to an end.

$$I \xrightarrow{h\nu} I^* \rightarrow R^* \quad \text{(initiation)} \tag{1}$$

$$R^* + M_1 \rightarrow RM_1^* \tag{2}$$

$$RM_1{}^*+M_2 \rightarrow RM_1M_2{}^* \tag{3}$$

$$RM_1...M_n{}^*+M_k \rightarrow RM_{(n+k)}{}^* \quad \text{(propagation)} \tag{4}$$

$$RM_{(n+k)}{}^*+R^* \rightarrow RM_{(n+k)}R \quad \text{(termination)} \tag{5}$$

$$RM_n{}^*+RM^* \rightarrow RM_nM_mR \quad \text{(termination)} \tag{6}$$

Usually, depending on the concentration and the photo-initiator type, the commercially available photoresist materials have a high absorption for the UV photons and are highly transparent to NIR radiation. The photo-initiator molecule excitation can be realized using the energy from UV photons or by two IR photons absorption. The non-linear optical effect of the two photon absorption (TPA), represents the rule behind the Two Photon Photopolymerization (TPP) method, where 3D structures can be realized deeply in the photoresist volume.

2.2. Two-Photons Absorption (TPA) effect

Two-photons absorption process was early emphasized in 1965 [23] using a ruby laser focused in a styrene and p-isopropylstyrene photoresist. The importance of this method was proved when a 3D spiral coil microstructure was created in SCR 500 (urethane acrylate) by an infrared femtosecond laser [24].

Like other commercially available photoresist materials, the SCR 500 was developed for UV lithography. Under specific conditions, the photo-polymerization mechanism can be initiated by infra-red photons. The probability to obtain the photo-polymerization effect using IR photons strongly depends on the radiation intensity. A much higher photon density is necessary compared with the UV exposure. IR lasers which work in continuous wave (CW) regime can not achieve this high density without inducing thermal damages in material. For this reason, low energy short-pulses IR lasers are tightly focused in the photoresist volume. When a femtosecond laser pulse is focused in the photoresist volume, high power density can be reached. In the central area of the focused laser beam, the photo-polymerization effect is induced in a very tiny volume (voxel). The voxel dimensions, that can be smaller than the size of the focused spot, correspond to the TPA volume (Figure 1).

By translating the focused laser spot through the photoresist volume, complex 3D microstructures can be obtained (Figure 2a). The voxel size and geometry can be modified by controlling the laser intensity or by using focusing optics with different numerical apertures (NA). Depending on the geometry created in the photoresist material, the NA of the focusing optics can be selected in order to control the axial resolution. The voxel shape is defined by an ellipsoid with a long axis d_z, which represent the axial resolution, and a short axis d_{xy}, which is the voxel thickness (Figure 2b).
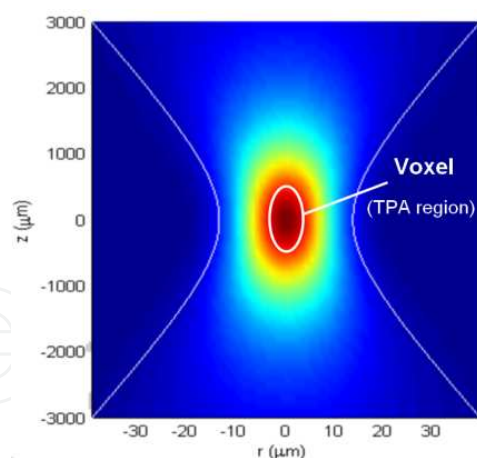
Figure 1. Longitudinal beam profile of the laser waist and the photopolymerized volume (voxel).
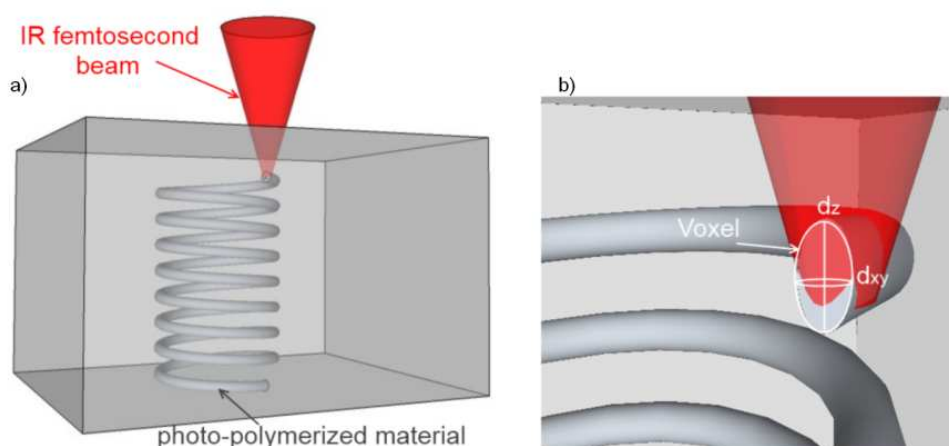

Figure 2. a) The sketch of the 3D structuring inside the transparent photopolymer. b) The geometry of the photo-polymerized voxel.

The voxel dimensions are also related to the photo-initiator used in the chemical composition of the photoresist material. Used in TPA processing method, the photo-initiator absorption efficiency is defined through a cross-section value (δ). Commercially available photoresists used in UV exposure are not created specially for the TPA processing. The low δ value of this processing method implies an increasing of laser energy and time exposure [25,26]. New photoresist materials with photo-initiators adapted for laser processing such as IP-L (Nano-scribe) were developed in order to obtain higher δ values.

This necessity generates new applications like up-converted lasing [27], where molecules with a large TPA cross-section are used. Several methods can be used to measure the δ value and to evaluate the TPA photo-initiators [28-30]. The elongation ratio value (d_z /d_{xy}) depends on the NA and can be reduced to 1.5 – 3, when focusing optics with high NA (~1.4 NA) are used. This NA value can be obtained only with immersion oil/water microscope objectives where the lateral spatial resolution can be less than 100 nm [31]. For smaller elongation value, shaded-
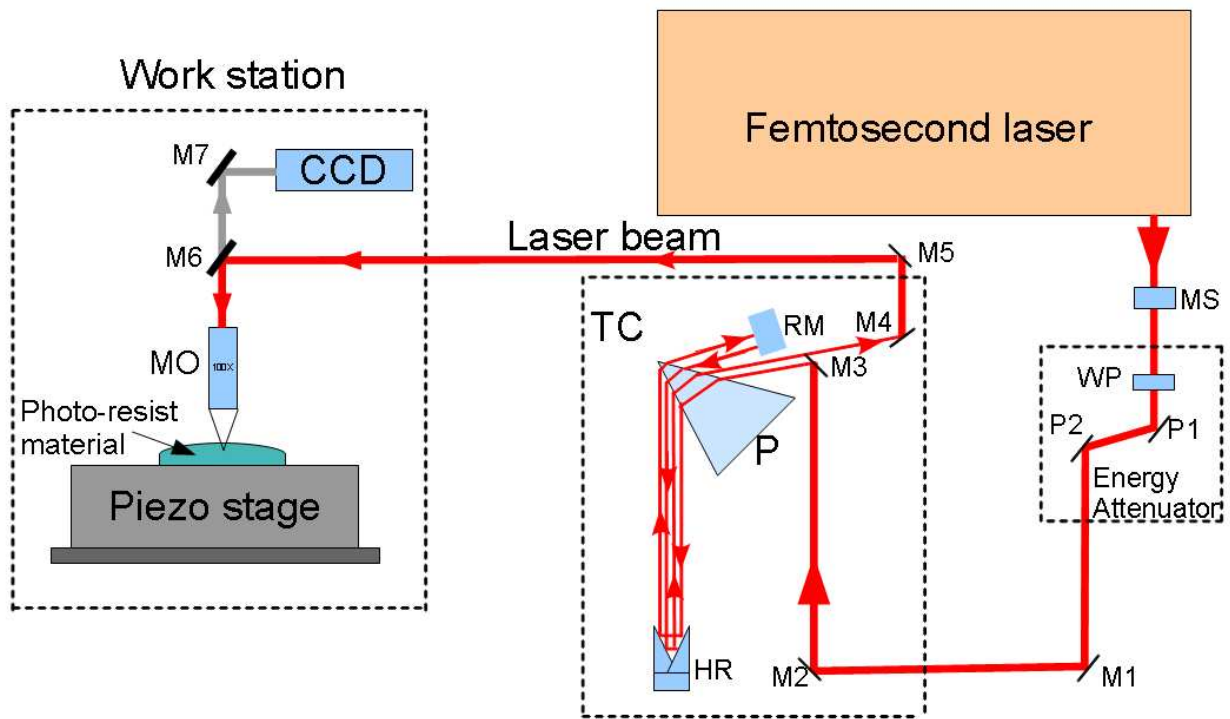
Figure 3. Schematic diagram of the DLW setup for 3D microprocessing using temporal compressor (TC): MS - Mechanical shutter; WP - Half wave-plate; P1 and P2 - Reflection Polarizers; P - BK7 prism; HR - Hollow Retro-reflector; RM - Roof Mirror; CCD - video camera; MO - microscope objective; M1 to M7 - Steering mirrors; M6 - Dichroic mirror.

rings [32] or annular binary filters [33] can be used to control the axial component (d_z) of the intensity distribution.

2.3. Experimental setup

A common Direct Laser Writing (DLW) setup for processing photoresist materials consists of the femtosecond laser source with high repetition rate, the attenuator for controlling the laser intensity, the focusing optics and translation stages with displacements at submicrometer resolution or better. For the 3D microstructuring experiments (Figure 3), a femtosecond laser oscillator with 5 nJ pulse energy, 15 fs pulse duration and 80 MHz repetition rate at 800 nm central wavelength was used. In order to preserve the laser pulse duration, the optical components of the experimental setup must be designed for a spectral bandwidth larger than 100 nm. Silver coated broadband optics were used for laser beam steering.

Positive group delay dispersion (GDD) generated by the glass in the optical path (focusing optics, polarizers, waveplates, beam colimators) produces a stretching of the pulse duration of the order of few hundreds of femtoseconds up to picosecond range. The temporal broadening of the pulses implies a considerable reduction of the laser peak power, leading to reduction of the photo-polymerization efficiency. In order to recover the pulse duration, for spectrally broad femtosecond laser sources, a dispersion compensator has to be used. The pulse chirp and pulse duration is controlled by tuning the GDD. In a standard dispersion compen-

sator with prisms, four or two prisms are used, with total length of the beam path up to few meters. For minimizing the set-up foot-print, the compensator can be folded by a hollow corner cube reflector (HR) and a roof mirror (RM) [34]. The femtosecond laser beam passes four time through a BK7 single prism. By changing the distance between the dispersive prism and the hollow reflector, variable GDD is introduced. In this approach, the temporal compression can be adjusted in a flexible way, even if the focusing optics or other optical components are changed in the optical path. The laser intensity is adjusted by a variable attenuator, which consists in a half wave-plate and two reflection polarizers.

For processing the photoresist, the laser was coupled with a work station realized in a modular configuration. The work station consists in focusing optics, sample translations with piezo and motorized stages, and the visualization module. The focusing optics were selected depending on the resolution and the desired working distance. A 100x IR Mitutoyo microscope objective with 0.5 NA and 12 mm working distance was used for microfabrication of high-aspect-ratio structures [35]. For sub-micrometer feature size, a 100x Zeiss oil immersion microscope objective with NA 1.4 is more appropriate. However, the total high of the structures is limited by the short working distance of such objective of 0.17 mm.

The photoresist samples are translated by a piezoelectric translation stage with 300 μm displacement on all XYZ axes. A software controls the scanning path, scanning speed and the laser shutter according to a programmed design. Pre-defined geometries can be selected from a library, or can be imported in stereolithography (STL) format. A CCD camera is used for monitoring the laser focus on the sample surface and for direct observation of the irradiated area during the laser processing.

The CCD camera can be replaced by a photomultiplier, or by a spectrometer for spectroscopy measurements working with the focusing optics in confocal regime. Using the above presented DLW setup, both organic photoresist materials and non-organic materials (chalcogenide glasses) were processed.

2.4. Processing protocol for organic materials

When photoresist materials are used in micro-device fabrication, a processing protocol including some steps has to be followed. Substrate cleaning, photoresist deposition, material exposure, and development are the main stages (Figure 4).
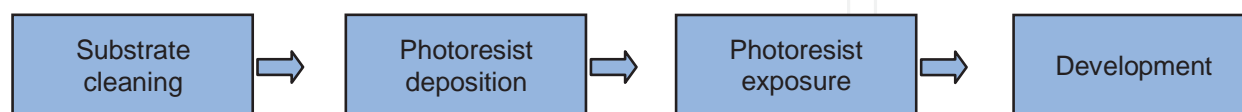

Figure 4. Usual process flow for the organic photoresist materials.

2.4.1. Substrate cleaning

Micro and nano processing technologies require a rigorous impurities control in order to prevent the sample contamination with dust particles or other chemical elements. The wafer

substrate cleaning represents one critical stage. Here, several procedures have to be carried out for a good adhesion between photoresist material and substrate. First, a ultrasonic bath with chemicals solvents, like acetone or piranha solution, is used to remove the impurities from the substrate surface. Then, the substrate is rinsed in pure deionised water in order to eliminate the remaining solvent. After this stage, water molecules are left on the substrate surface, inducing a weak photoresist adhesion to the substrate. A water desorption step, which can be realized by heating the substrates to 150 ºC for 30 minutes or using oxygen plasma cleaning, is necessary. The photoresist adhesion to different substrates can be poor, even if the water desorption was performed. Several methods can be used to eliminate this drawback. Reactive plasma etching, chemical corrosion or adding a promoter adhesion layer can be used. These treatments are usually recommended by the photoresist manufacturer.

2.4.2. Photoresist deposition

The photoresist material can be deposited on the substrate using various methods. Spray-coating, spin-coating, drop-cast or roller-coating are few methods which can be used. The most used common technique is spin-coating. Characterized through uniform and thin film thickness, this method uses the spinning speed to control the photoresist deposition. In order to use this deposition method, the photoresist must be in a liquid state. For this reason, the viscosity of the photoresist material is controlled using chemical solvents. For different viscosities, photoresist manufacturers provide informations about the evolution of the film thickness reported to spin rate (rpm) and time (s). Varying the ratio between the solid content and the solvent, photoresist materials can be deposited from 1 μm up to 1 mm.

One of the most popular negative photoresists, SU-8, is an epoxies based material where the polymerization is done by a cationic photo-polymerization mechanism. For this material a wide range of viscosities can be found. When the required thickness of the film is less than few micrometers, the manufacturer recommends to use a photoresist version which has 40% solid content and 60% solvent. For this viscosity, 1 ml of liquid SU-8 is necessary for every inch diameter of the substrate. The distribution of this quantity on the substrate surface begins with low spinning speed (500 rpm) for few seconds. Then, the speed is increased up to 8000 rpm in order to obtain 1 μm film thickness.

After deposition stage, for some photoresist materials a soft bake step is required. For SU-8 material, a thermal treatment was performed. A hot plate heated at 95⁰ C is recommended to be used. During this step, the solvent is eliminated from the material, resulting a solidified material. A baking time ranging from 2-3 minutes for 4-10 microns photoresist thickness up to 15-40 minutes for 40-100 microns thickness is required. Because an insufficient thermal treatment could create a weak adhesion to the substrate and deformed structures, this step is very important.

2.4.3. Photoresist exposure by IR femtosecond lasers

The dimensions of the photoresist structures produced through TPP method depend on the focusing optics and processing parameters like fluence and scanning speed. The importance

of the focusing optics, especially the NA, to voxel shape has been detailed in subsection 2.2. Here, the importance of the fluence and the scanning speed will be emphasized. These two parameters control the dimension and strength of the photoresist structures. Usually, in order to determine the most suitable conditions, a processing map is plotted for a given fluence F and different scanning speeds. The process is repeated for different fluence values (e.g. 2F, 3F, …, nF). In this way, through combinations between scanning speed and fluence, photoresist structures with different thickness are produced (Figure 5). After the imprinted pattern is investigated, the optimum exposure conditions are selected.
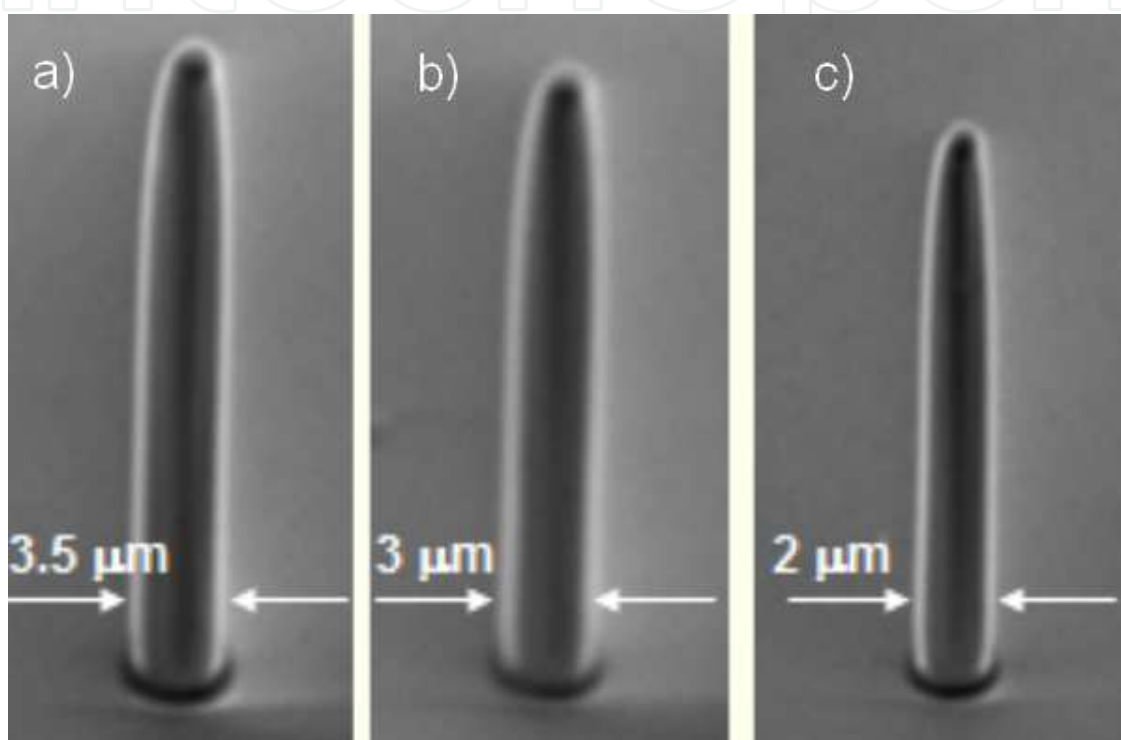

Figure 5. Pillars realised in OrmoComp photoresist by translating the IR focused beam (SynergyPro oscillator) in Z directions with different scanning speed. The fluence was fixed at 8.9 mJ/cm^2 and the scanning speed was : a) 5 μm/s b) 10 μm/s c) 50 μm/s.

In the SU-8 photoresist case, after exposure, the refractive index difference between the exposed and unexposed area is very low due to the fact that the polymerization is not realized instantaneously during exposure. In order to complete the formation of the polymeric chains, a supplementary post-exposure bake step is required.

Unlike the SU-8, the Ormocers and OrmoComp hybrid photoresists are laser photo-polymerized in a single irradiation step, without any additional thermal treatment. In these classes of inorganic-organic hybrid photoresists, the polymerization is instantly produced.

After exposure, for all photoresist materials a chemical etching stage is performed. Depending on the photoresist type, different chemical solvents are used to remove the exposed or unexposed photoresist material.

2.4.4. Development stage

When the photo-polymerization mechanism is accomplished, chemical solvents are used to develop the sample. Two classes of photoresists are identified: positive and negative. In the negative photoresists case, the irradiated material is transformed in polymer chains and becomes insoluble to solvents. Therefore, the non-irradiated material is removed. Unlike negative photoresists, the positive irradiated photoresists become soluble, being removed by the solvent.

2.4.5. Limiting factors in organic photoresist processing

Photoresist materials developed for nano-processing lithography have to satisfy several conditions in order to be used for MEMS mass production. The physical and chemical material properties, temperature conditions storage, chemical reactions with other materials, film thickness, minimum dot size, etching rate, are important parameters for semiconductor industry. Besides these parameters, other limiting factors are encountered in photoresist materials processing.

One limiting factor, which can induce some deviations from the initial design, is the shrinkage effect. Due to the photoresist chemical properties, the shrinkage effect appears after the etching stage where the structure becomes temporally a swollen gel. After complete removal of the solvent, the volume of the structure reduces and the initially designed opto-mechanical characteristics are changed. The shrinkage effect can be pre-compensated by adjusting the initial design of the structure. This way, a final photoresist structure with the desired symmetry and dimensions can result after the shrinkage. An attenuation of the shrinkage effect can be also obtained by developing new improved photoresist materials or by adjusting the photo-resist protocol [36].

Even if the shrinkage was compensated, another limiting factor can appear after chemical etching. Here, the microstructures created are stand alone, immersed in the solvent. During the sample extraction from solvent, the capillary forces can induce pattern distortions. To avoid this, methods like super-critical drying (SCD) [37] or the change of the contact angle between the structure and solvent during extractions were used [38].

2.5. Applications of the organic photoresist microstructures

2.5.1. High power laser targets

Several materials (e.g Zr, Mo, Au, Ag, Al) can be used as laser targets in experiments like fast ignition [39], X-ray emission [40], shock compression [41], ion acceleration [42] or hot electrons generation [43]. When a high power laser pulse interacts with a material, due to the strong electromagnetic field, hot dense, highly ionized plasma is generated. The resulted electrons, protons, ions or X-rays are analysed and used in many applications. Concepts of fusion or fast ignitions lead to new targets geometry, where the properties of the emitted particles like energy and directionality are analysed and improved. Using micro-cones target geometry, highly charged and collimated particles were produced through a better coupling between laser

energy and material. Plasma structuring and optimization of radiation emission [44], represent two advantages of the new targets geometry. When the thickness [45] and lateral dimensions [46] of the target are reduced, the proton energy and the laser energy conversion efficiency increase.

With a sub-micrometer resolution, the photoresist materials offer an alternative to conventional high power laser targets fabrication methods. Using a microscope objective with 0.5 NA, capillary microstructures were created in Ormocore material through TPP method (Figure 6). Keeping the IR femtosecond beam focused on the substrate surface and by translating the sample, capillary structures with reduced height and thickness were obtained (Figure 6a). The capillary height can be increased by translating the focused beam along the Z axis through the photoresist volume (Figure 6b).
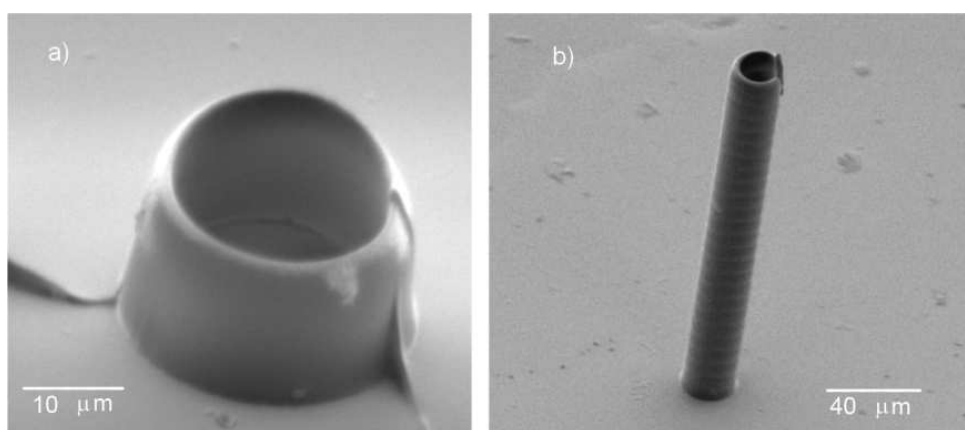

Figure 6. Capillary microstructures obtained in Ormocore photoresist by TPP method.

The photoresist structures can be used as template for more complex geometries. Other materials like metal or ceramics can be afterward deposited on the photopolimerised structures by different techniques, such as electroplating, thermal evaporation, pulsed laser deposition. After deposition, the photoresist material is eliminated by thermal treatment. The final target will reproduce the photoresist microstructure design.

2.5.2. Light coupling masks

Other applications of photoresist microstructures are in the optical contact lithography [47] and laser interference surface processing [48]. In both cases, a transparent photoresist mask with a periodic pattern is used to change the electromagnetic field propagation, generating a phase-shift during the propagation through the mask. Due to the periodic phase-shift introduced by the mask, an interference pattern is obtained. If the mask is placed in the proximity of a sample, the interference pattern and the localized high laser fluence induce modifications on the surface of the material or even inside the transparent photoresists. Initially used for photoresist processing, where sub-wavelength photoresist structure were produced, this method was implemented for semiconductor processing too.

We created a photoresist mask in a PMMA positive photoresist for light coupling mask (LCM) experiments. Using the spin-coating method, a photoresist layer with 300 nm thickness was deposited on a glass substrate. The photoresist mask, with a grid pattern periodicity of 2 μm, has been created by electron beam lithography (Figure 7a). We placed the photoresist mask in contact with a silicon wafer, without any additional pressure.

The mask was irradiated by an IR femtosecond laser pulse (775 nm central wavelength, 200 fs pulse duration) through a focusing lens with 75 mm focal length (Figure 7b). The laser fluency on silicon surface was 0.15 J/cm^2, below the silicon ablation threshold. Due to the electromagnetic field enhancement under photoresist mask, the laser fluency was enough to locally ablate the silicon wafer. Periodic grooves with 350 nm width and few nm depth, were obtained on silicon wafer surface (Figure 8). The imprinted pattern is identical with the configuration of the mask. In order to imprint a large area, the size of the spot was increased by changing the focus position with 1 cm below the photoresist mask position (Figure 7b).

A large silicon wafer surface was structured with a single IR laser pulse (Figure 9). Both the photoresist mask and the imprinted pattern were investigated by Atomic Force Microscopy (AFM).

Because the exposed area dimensions are limited only by the laser available energy and not by the photoresist mask, this method represents a fast and low cost surface processing technology.
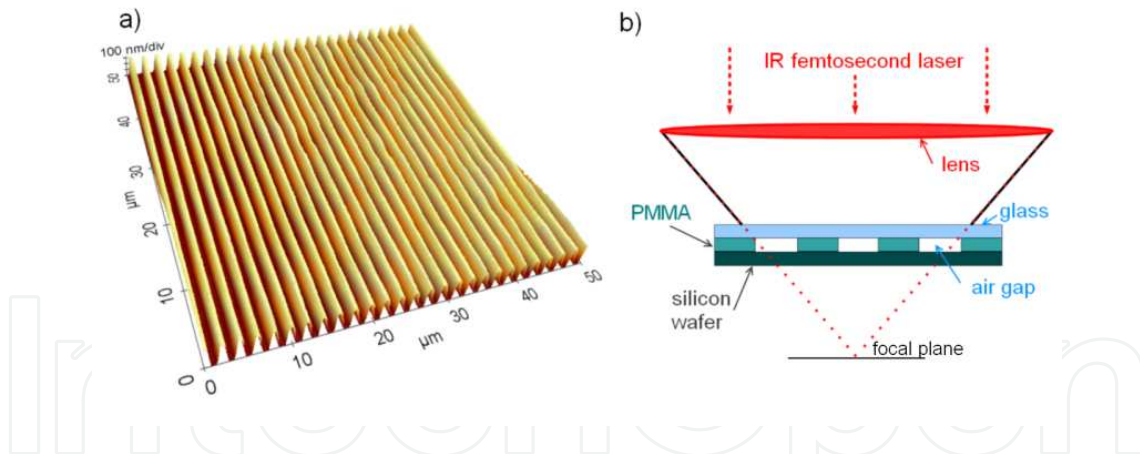

Figure 7. Large areas processing using LCM. a) The 3D AFM image of the PMMA photoresist mask. b) The experimental setup for large area processing.

2.5.3. Photonic nanostructures

The actual computing speed of the micro-processors is limited mainly by the resistive heating resulting from the electrons current in circuits and it is hard to be improved. To overcome this limitation a new technology which uses light instead of electrons is foreseen. A photonic device will provide a fast signal processing, transmission of higher information volume and lower power consumption.
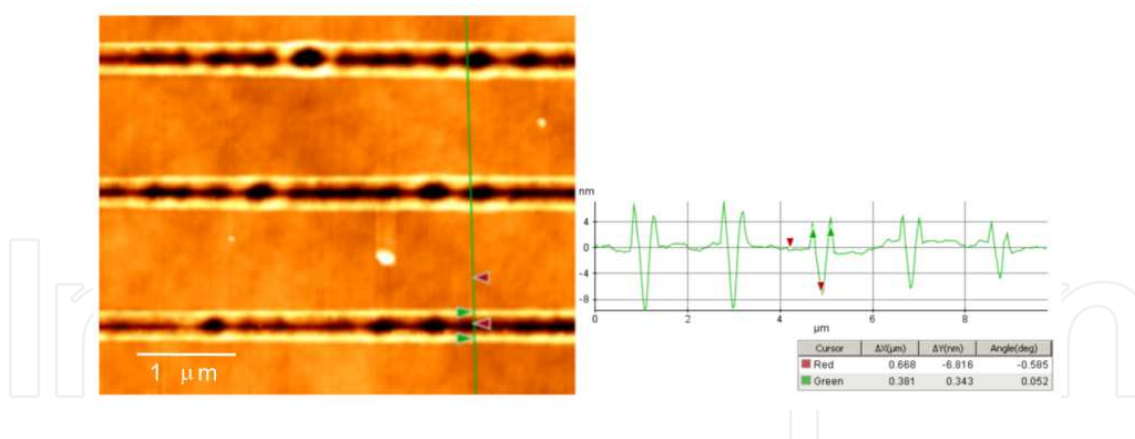
Figure 8. AFM image and profile of the periodic grooves imprinted in silicon wafer using LCM.
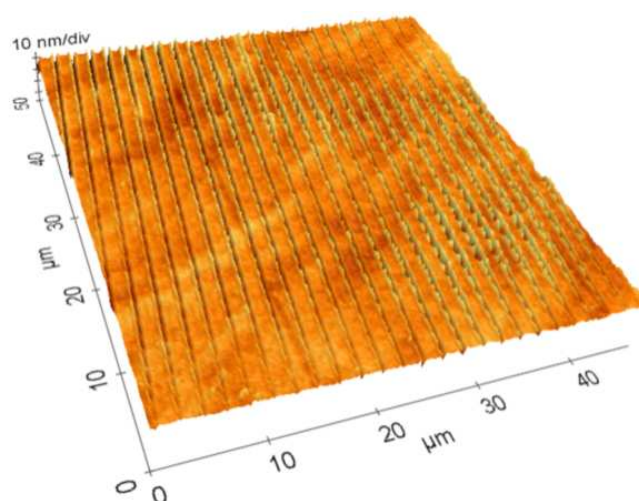

Figure 9. Extended area of imprinted pattern on silicon surface using LCM.

In such devices the propagation of the light is controlled by the so called photonic bandgap structures. These structures usually consist of periodic arrangements of photonic "atoms" with designed voids or defects such as cavities, or waveguides. The dimension of the photonic "atoms" and the period of the photonic structures are comparable with the light wavelength. Special designs and material configurations could even lead to non-conventional optical effects such as negative refraction index, negative refraction, cloaking at visible frequencies. The structures presenting such fascinating effect are widely known as negative index metamaterials (NIM). The dimension of an elementary cell in a metamaterial is several times smaller than the light wavelength and could decrease down to 100 nm for optical frequencies. For this reason, the fabrication of the photonic bandgap structures and metamaterials for visible spectral range requires complex processing techniques which are able to generate 3D structures with dimensions of the order of few hundreds nm and even below 100 nm. DLW is one of these techniques providing high accuracy in 3D. Such processing equipments are already commercially available for producing 2D and 3D structures with minimum linewidth of about

100 nm. Using a 3D lithography system (Photonic Professional - Nanoscribe) based on TPP, we have obtained structures with dimensions of 90 nm (Figure 10a). A scanning speed of 50 µm/s and a 0,1 nJ pulse energy at 80 MHz repetition rate were used to create a periodic pattern. An immersion oil microscope objective 100x and 1.4 numerical aperture was used for focusing the pulsed laser beam in the comercial photoresist IP-L (Nanoscribe), specially developed for TPP method.
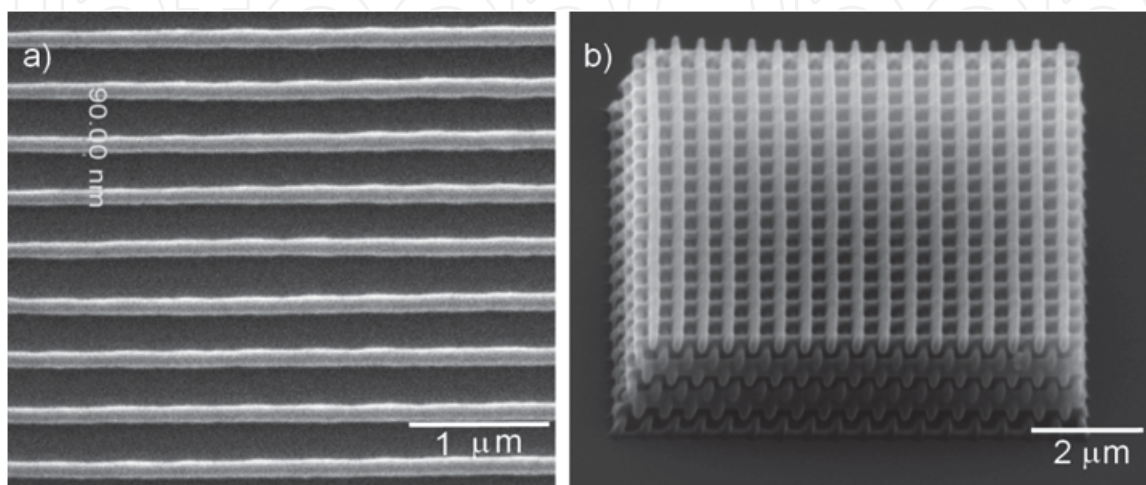

Figure 10. Nanostructures produced in IP-L photoresist. a) periodic lines; b) woodpile structure.

The organic materials have low refractive index, usually at the order of 1.4-1.6 at the visible wavelengths. In simple geometries, such as periodic arrangements of pillars in hexagonal or rectangular symmetry, the structures will not show photonic bandgaps. Complex geometries such as woodpiles has to be designed. 3D structures can be obtained by scanning the photoresist layer by layer. Recently, we have fabricated a woodpile structure with a period of 500 nm between lines and 5 µm tall (Figure 10b). For this value of the period, these structures could show photonic bandgaps for the visible spectral domain.

An alternative solution to these complex designs is to realize microstructures in non-organic photoresist materials, like chalcogenide glasses, with higher refractive index.

3. Laser processing of non-organic materials

3.1. Non-organic photoresist materials

The chalcogenides are materials either in crystalline or amorphous states, which are based on the chalcogen elements (Sulphur, Selenium and Tellurium) in combination with other elements (Arsenic, Phosphorus, Germanium, Tin, etc.). The structure of the chalcogenides is based on a network of covalent bonds, which gives the specific properties to these materials. While the crystalline state of the chalcogenide can be hardly obtained, the amorphous phase can be easily obtained by the melt cooling [49].

The properties of the amorphous (glassy) compositions are quite different from the crystalline counterparts. The basic structure at the atomic level consists in chains of atoms for elemental chalcogen and disordered layers for complex chalcogenides. A typical chalcogenide structure (Arsenic trisulphide, As_2S_3) in a bulk glass is shown in Figure 11a, while a disordered layer is presented in Figure 11b. Arsenic trisulphide glass is intensively studied due to its optical properties and versatility in structural modifications. It is characterized by a high nonlinear refractive index (Figure 12a), high transmission in infrared regions, and low phonon energies.

The study of the optical features of non-crystalline vitreous semiconductors near the absorption edge is of great interest. The absorption edge of non-crystalline materials is very sensitive to material composition and structure as well as external factors such as electric and magnetic fields, heat, light, and other radiation. Under the influence of these factors the optical properties of non-crystalline semiconductors are reversible or irreversible modified. They are suitable for optical investigations because their absorption edge is in the visible region of the spectrum. The absorption edge of As_2S_3 is at 2.4 eV (Figure 12b). Moreover, vitreous materials can be easily obtained in bulk samples, thin film, and optical fibers. These properties make them suitable to be used as materials for components in optoelectronic devices, as solid electrolites, photonic crystals, IR-transmitters, optical and electrical phase change memories or rewritable memory materials for CD's and DVD's.

Due to their sensitivity to different radiation wavelengths, chalcogenide glasses are suitable for laser lithography. They have small molecular units thus having the possibility to obtain higher resolution. They are much harder than polymers and can maintain the shape.

Due to the metal photodissolution in chalcogenide glasses, dry grayscale lithography can be done [50,51]. Chalcogenide glasses can also be used for wet lithography. Much simpler etching can be done without any treatments and they are resistant to acids. Thereby, there is easy to transfer patterns in substrates using reactive ion etching.

Depending on the type of glasses, both positive and negative resists can be obtained. Besides currently available organic photoresists, chalcogenide glasses offer a new powerful class of photoresists for a versatile lithography.

3.2. Light interaction with chalcogenide glasses

Many applications of the glassy chalcogenides are based on their interaction with light. Recently, different effects produced in chalcogenide glasses and thin films were investigated [52]. The main effects related to the interaction of the light with the glass are:

- Photodarkening and photobleaching

- Photoexpansion of the material

- Change of composition with the elimination of one chalcogen

- Vaporization of the material

The photodarkening [53 - 57] and photobleaching [58] effects were the first optical effects discovered in chalcogenide glasses. The optical absorption edge can be shifted toward higher
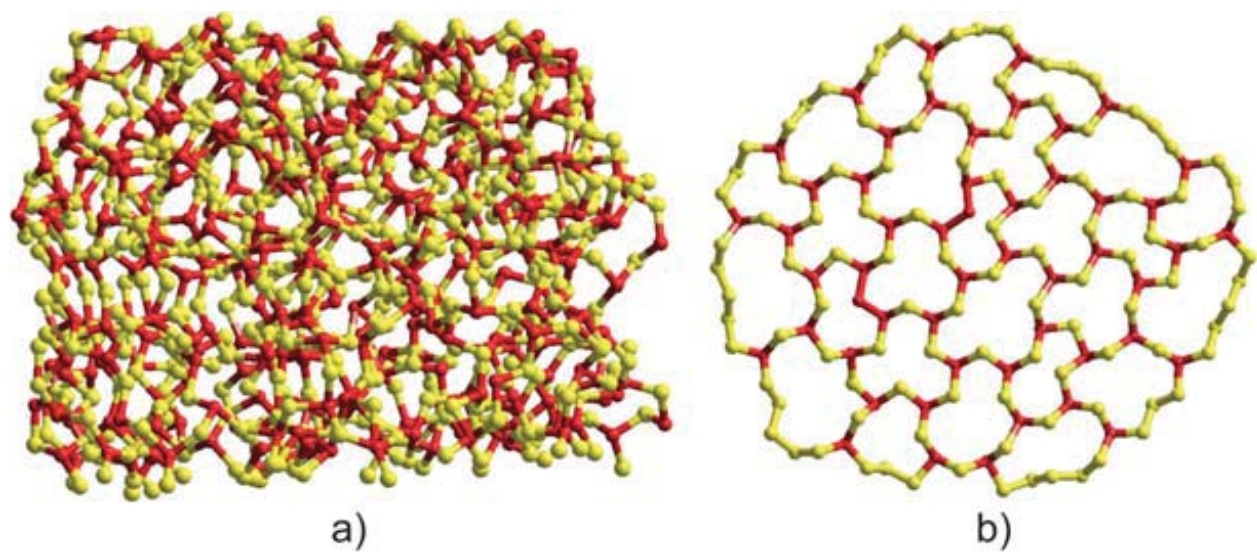
Figure 11. a) The structure of As$_2$S$_3$ glass in a bulk glass. b) A thin disordered film. (As – red, S – yellow)
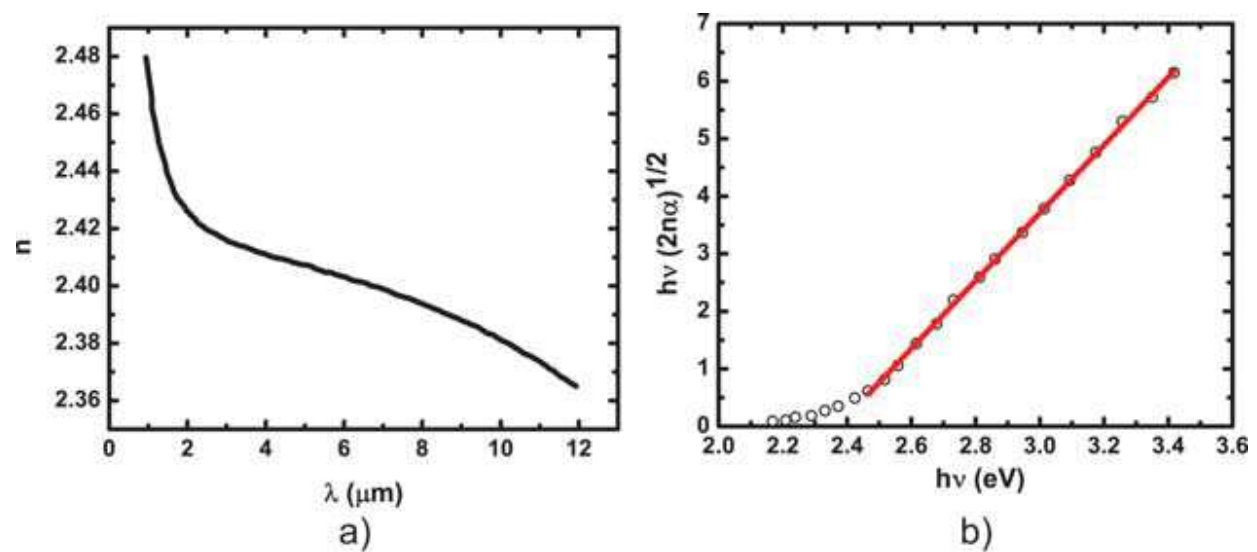

Figure 12. Optical properties of As$_2$S$_3$ glass. a) The variation of the refractive index with the wavelength. b) The absorption edge.

wavelengths (photodarkening) or toward lower wavelengths region (photobleaching) under laser light illumination with photon energy near absorption edge (2.4 eV). These processes are reversible as a function of heat treatment (under the glass transition temperature (T_g)).

The photoexpansion is one of the main phenomena which produce photoinduced volume change. The irradiation of amorphous chalcogenides films with bandgap light produces an increase in thickness and is termed photoexpansion [59, 60]. It has been demonstrated that amorphous As$_2$S$_3$ thin films irradiated with bandgap and sub-bandgap light expand with about 0.5 % and 4 % (giant photoexpansion) [61], respectively. Both photoexpansion and giant photoexpansion vanish after annealing close to the glass transition temperature. On the other

hand, when the material is irradiated with super-bandgap light, photocontraction effects ascribed to ablation or photovaporization [62] are induced. Photoexpansion and photocontraction are usually produced in chalcogenides, the sign of the effect depending on the glass composition [63 – 68].

One important effect occurring during interaction of high power light with the chalcogenide material is the vaporization in the chalcogenide mass. The vaporization occurs by elimination of clusters of different composition and size [69]. Vaporization is preceded by photofluidity effect discovered by Hisakuni and Tanaka [70]. The standard processing protocol of a chalcogenide photoresist is described in the next section.

3.3. Processing protocol for chalcogenide glasses

As shown in the previous section, chalcogenide materials have specific properties that make them suitable for lithography. The steps of the lithographic process in chalcogenide glasses are presented in Figure 13. First, a chalcogenide thin layer is deposited on a glass substrate using the pulsed laser deposition method (PLD). As_2S_3 films were deposited on glass substrate by PLD using a KrF* excimer laser, with 80 mJ pulse energy and 25 ns pulse duration at 248 nm wavelength. Homogeneous films were obtained with thickness of around 2 micrometers. Secondly, the layer is irradiated using femtosecond laser pulses (λ = 800 nm).
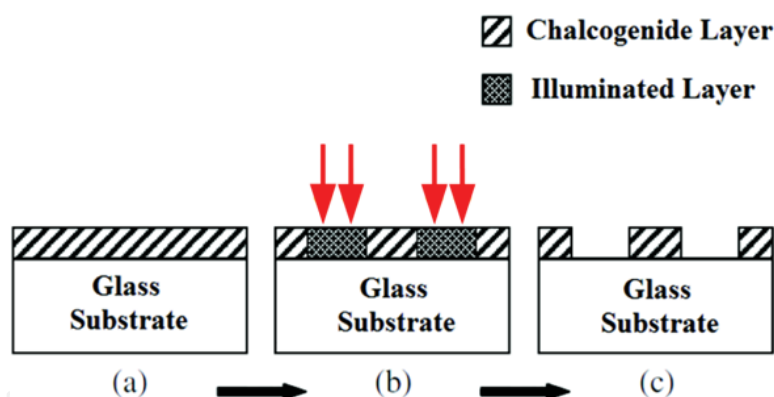

Figure 13. The lithographic process in As_2S_3 chalcogenide glass.

In this case the chalcogenide glass acts like a negative photoresist. In the final step, the sample is etched using an amine based aqueous etchant. The removal of the irradiated regions by etching leaves behind the selected regions of the photoresist. In the following subsections we present the main methods used for chalcogenide glasses processing using laser irradiation: direct laser writing by pulsed femtosecond laser irradiation and interference lithography.

3.3.1. Pulsed femtosecond laser irradiation. Two photon absorption in chalcogenide glasses

It is known that the chalcogenide glasses exhibits a characteristic one-photon absorption spectrum. The absorption edge consists of three functional curves, i.e., a square-root dependence, the so-called Urbach edge, and an exponential weak-absorption tail. The weak-absorp-

tion tail limits optical transparency of chalcogenide glasses [71]. The two-photon absorption spectrum of As_2S_3 glass has an exponential form $\beta = \exp(h\omega/E_\beta)$, where $E_\beta \sim 150$ meV [72].

This exponential form implies that the two photon process is enhanced by the gap states, which cause the weak-absorption tail. When the incident light intensity is less than 10 MW/cm², one-photon excitation of the gap states occurs more frequently than two-photon excitation of free carriers, and accordingly, the former could be responsible for the phenomena photoinduced by sub bandgap photons.

From the studies of the 3D optical data storage into As_2S_3 blocks via photodarkening with 800-nm femtosecond laser pulses [73] it was shown that two photon absorption can be achieved using relatively low energy laser pulses. The two-photon absorption cross-section was found to be 6.2 ± 0.5 GM (Goeppert-Mayer units, where 1 GM is 10^{-50} cm⁴ s photon⁻¹) at around 800 nm wavelength.
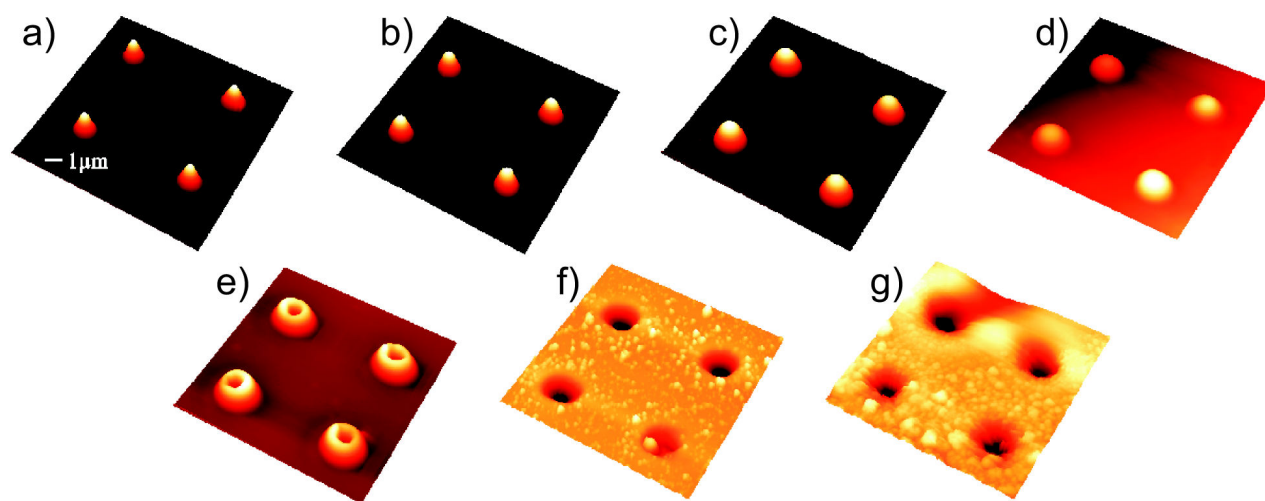

Figure 14. AFM images of laser irradiated As_2S_3 thin film surface using an average laser power of a) 8 mW, b) 12 mW, c) 18 mW, d) 20 mW, e) 25 mW, f) 30 mW, g) 50 mW

Some results of femtosecond laser imprints on As_2S_3 film surface have been reported in reference [74].

Using a femtosecond laser with 80 MHz repetition rate and 15 femtosecond pulse durations, a network of nano-lenslets was created by local exposure of individual sites separated by 5 µm × 5 µm. The irradiation was performed for 300 ms in each point. The average laser power was varied from 8 to 50 mW, corresponding to femtosecond pulse laser energy from 0.1 nJ to 0.63 nJ.

In Figure 14, one can see the formation of hillocks and/or holes on the surface of a thin amorphous As_2S_3 film by direct laser writing method using femtosecond laser pulses (central wavelength, $\lambda_c = 800$ nm). The shape of the modified surface is found to be a function of the laser power. Thus, a network of nano-lenslets could be imprinted at appropriate laser power and might be used in planar optoelectronic circuits.

It can be observed a boundary between the low energy laser pulses and high energy laser pulses. For low energy laser pulses the main evidenced effect is the photoexpansion. For higher energy pulses, over 0.25 nJ, a process of material ablation takes place and determines the holes formation into the film.

3.3.2. Interference lithography

Interference lithography (IL) is widely used for the fabrication of one dimensional nanostructures [75], production of the master mold for nano-imprinting lithography [76], formation of grating structures on semiconductor surfaces [77,78], pre-patterning of the substrate before the formation of photonic crystals by electrochemical etching [79] or vacuum deposition [80] etc.

We used As_2S_3-As_2Se_3 as an inorganic photoresist for the fabrication of submicrometer periodic relief on silicon wafers using interference lithography [81]. A 300 nm thick photoresist of As_2S_3-As_2Se_3 was vacuum evaporated on a (100) silicon substrate on which a 50 nm thick chromium layer was previously deposited. The obtained samples were exposed to an interference pattern that was generated by an argon laser (λ = 488 nm) using a holographic setup. To generate interference fringes, light beam has to be divided into two waves which afterwards are recombined. In an amplitude-division system, a beam splitter is used to divide the light into two beams travelling in different directions, which are then superimposed to produce the interference pattern. The laser fluence was around 0.5 J/cm². For the formation of bi-gratings each exposure can be 1.5-2 times reduced. The two-dimensional periodic structures on Si (100) surface were formed by double exposure on two perpendicular orientations of the Si wafers.

During the first exposure, Si (100) wafers were aligned by a base cut in parallel to interference grating lines and during the second irradiation the wafers were rotated with 90°. The size of the exposed part on the substrate reached up to 0,075 mm ▪ x 0,075 mm. ▪

After exposure, the samples were chemically treated in non-water alkaline organic solutions (negative etching) to form a relief pattern. The removal of Cr layer using water solution of HCl through a chalcogenide mask was the next step. Thus, the obtained two-layer resistive mask As_2S_3-As_2Se_3-Cr was used to form a corresponding relief on Si surface. Anisotropic etching of silicon was carried out using ethylene diamine solutions.

As ethylene diamine actively dissolves chalcogenides, etching of silicon occurred, mainly, through a Cr resistive mask that is neutral to alkaline solutions.

Figure 15a shows the AFM image of a diffraction grating formed on the silicon (100) surface by the anisotropic etching through As_2S_3-As_2Se_3-Cr resistive mask (grating period is near 1.0 µm). Figure 15b shows the bi-grating structure that was formed using double exposure of 0.3 J/cm². Symmetrical photoresist islands were obtained, with the ratio of the island diameter to the interval width between islands closed to unity. Time of the silicon etching was 15 s. Depth of the obtained relief is 0.15 micrometers. The size of photoresist islands depends on the value of exposure, and the form of islands depends on the ratio of exposures in two mutually perpendicular directions.
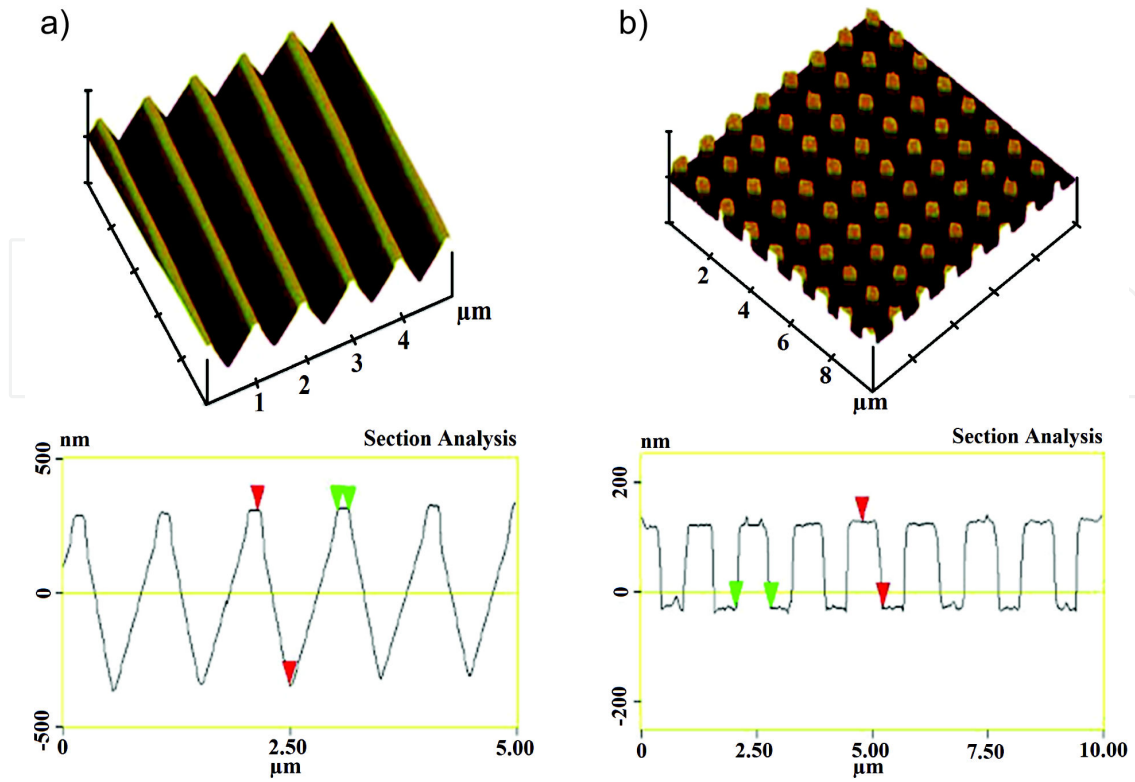
Figure 15. AFM images of the created relief on the surface of Si (100). a) Relief and groove profile of a grating obtained on by 50 s silicon etching. b) Profile of bi-grating with symmetrical elements obtained by a 15 s etching time.

Two applications of the lithographic process in chalcogenide glasses are presented in the next section.

3.4. Chalcogenide glasses applications

3.4.1. Optical microlenses

A first application is related to the formation of microlenslets on the surface of the chalcogenide film. By irradiating a thin chalcogenide film with the above mentioned femtosecond laser (Section 3.3.1), As_2S_3 microlenses were obtained. The profile of the lenslet measured from the AFM data was fitted with an asymmetric double sigmoidal curve (Figure 16). The fitting curve is given by equation (7), where y_0 is the offset, A is the amplitude, x_c is centroid and w_1, w_2, w_3 are width parameters.

$$y = y_0 + \frac{A \cdot \left(1 - \frac{1}{1 + e^{-\left(\frac{x - 0.5 \cdot w_1}{w_3} \right)}} \right)}{1 + \frac{1}{1 + e^{-\left(\frac{x - 0.5 \cdot w_1}{w_2} \right)}}} \tag{7}$$
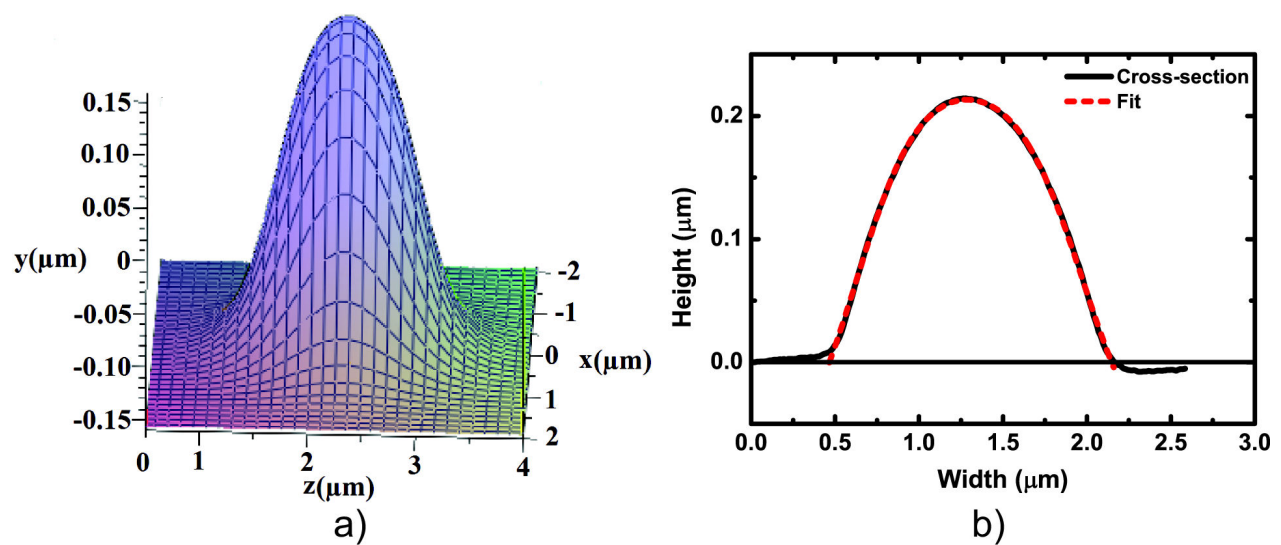
Figure 16. Chalcogenide microlenses. a) A lens represented by a 3D-plot. b) The shape of the lens fitted by an asymmetric double sigmoidal curve.

Fitting parameter	Value	Standard error
y_0	-0.09925	0.00382
x_c	8.30668	0.00035
A	0.33291	0
w_1	1.34572	0.00763
w_2	0.18998	0.00267
w_3	0.20191	0

Table 1. Fitting parameters

The lenslet profile is very well fitted to the parameters of the fitting curve presented in Table 1. The geometrical characteristics of the lenslet are: a diameter of 2.03 μm and a height of 0.21 μm. The focal length was between 1.21 μm at λ = 650 nm and 1.37 μm at λ = 5 μm (Figure 17). For computing the focal length we used the values of the refractive indices at different wavelengths from [82]. The transmission of light through the lenslets is limited by the As_2S_3 optical absorption edge of 2.41 eV.

3.4.2. Photonic crystals

Photonic structures are important components of the optoelectronic circuits used in telecommunications and in non-linear optics, as lossless guiding [83] and tightly bent 90° waveguides [84]. They can combine optical waveguides, resonators, dispersive devices and modulators for on-chip integration. Recently, it was shown that various 2D or 3D structures can be inscribed on the surface and bulk of an arsenic sulphide glass by the action of femtosecond laser pulses followed by etching in alkali or amine based etchants [85,86]. The laser installation is presented in section 2.3.
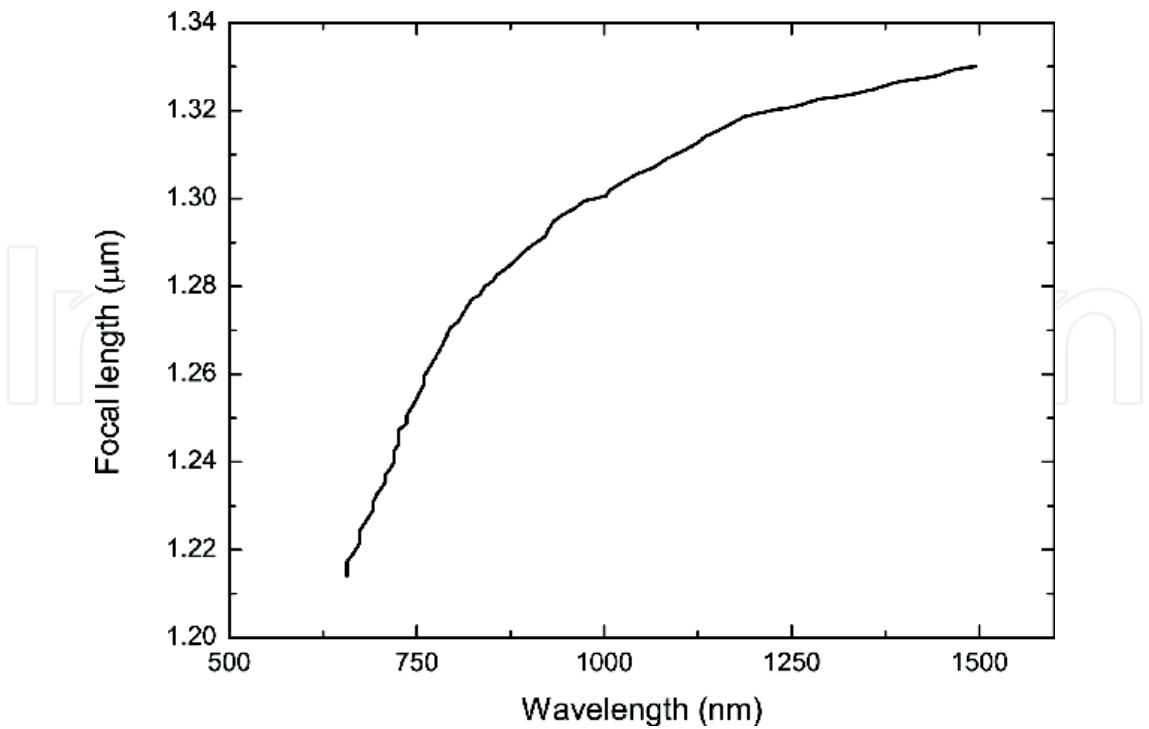
Figure 17. The variation of the focal length of the microlenslets with the radiation wavelength.

A 2D photonic crystal structure was imprinted on the surface of bulk As_2S_3 chalcogenide glass. Regular bumps obtained by photoexpansion of the glassy material have the height of $150 - 200$ nm (Figure 18a) [87].

After etching, using an amine based etchant, a hexagonal lattice of holes having the diameter of about 2 micrometers was obtained (Figure 18b).

In order to obtain photonic devices for the visible light domain, further investigations are in progress to improve the processing parameters.
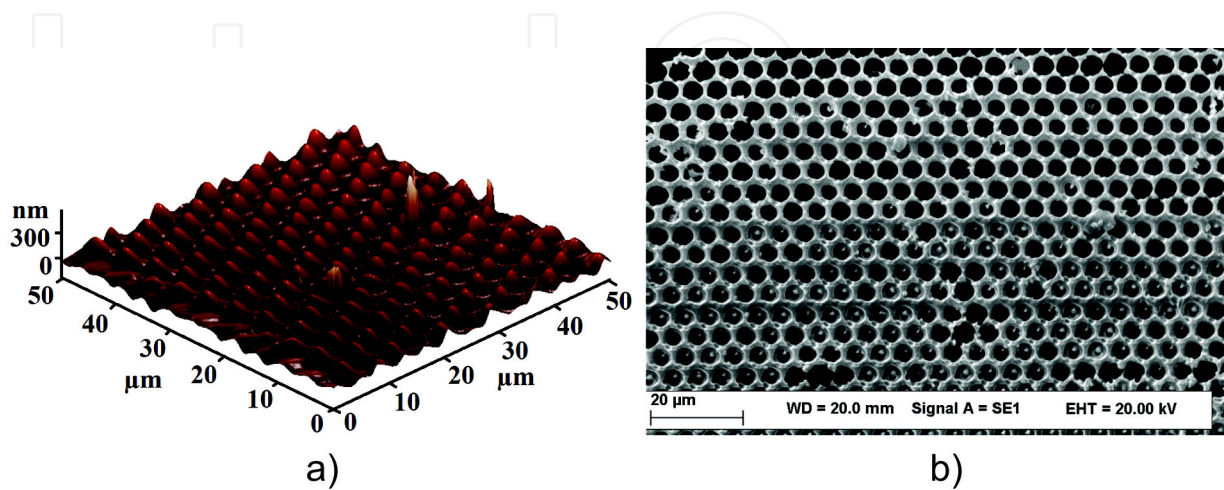

a)   b)

Figure 18. photonic crystal. a) Before etching. b) After etching.

4. Conclusions

The laser lithography can be considered an alternative to the classical lithography methods. In this chapter we emphasize the possibility to obtain nano/micro-structures in organic and non-organic materials by femtosecond laser lithography.

The organic and non-organic photoresist materials properties are presented. Photo-chemical reactions induced by femtosecond laser irradiation of photoresists are described. Due to the transparency at IR wavelengths, the laser pulses can be focused deeply in the photoresist volume. A Direct Laser Writing station coupled with a high repetition rate femtosecond laser was used to process the photoresist materials.

Various geometry structures were obtained in organic photoresists and chalcogenide glasses. When photoresist materials specially developed for the TPP method were used, nanostructures with dimensions under 100 nm were obtained.

Using the TPP method, high power laser targets were fabricated in organic photoresist materials. These structures can be used as template for other materials. An other domain where the organic photoresist structures can be used is optical contact lithography. Based on the electromagnetic field enhancement produced by the photoresist masks, structures with 350 nm width were created in a silicon wafer.

Besides the organic photoresists, the femtosecond laser lithography can be used to process other photoresist materials, like chalcogenide glasses. Taking advantage of their higher refractive index in comparison with organic photoresists, the chalcogenide glasses are suitable for visible and near-IR micro-optical devices fabrication. They act either as negative or positive photoresists. Optical microlenses and photonic crystals structures where produced in As_2S_3 chalcogenide glasses using DLW method. The microlenses imprinted on the surface of PLD deposited As_2S_3 thin films could be used to focus the red-infrared laser light transmitted through optical fibers. Transition from the bump to the hole configuration has been revealed when the laser pulse power was increased. Bi-dimensional photonic structures characterized by a hexagonal assembly of bumps or gratings with traces of micrometer width have been obtained.

The possibility of structure direct writing by translating the focused spot through the photoresists volume, recommends the femtosecond laser lithography technique as a fast, cheap and flexible processing method.

Author details

Florin Jipa[1], Marian Zamfirescu[1], Alin Velea[2], Mihai Popescu[2] and Razvan Dabu[1*]

*Address all correspondence to: razvan.dabu@inflpr.ro

1 National Institute for Laser, Plasma and Radiation Physics, Magurele, Romania

2 National Institute of Materials Physics, Magurele, Romania

References

[1]   Pilnam K. Soft Lithography for Microfluidics. A Review, BIOCHIP JOURNAL 2008; 2(1) 1-11.

[2]   Unger M. A, Chou H, Thorsen T, Scherer A, Quake S. Monolithic Microfabricated Valves and Pumps by Multilayer Soft Lithography. Science 2000; 288 (5463) 113-116.

[3]   Matsuyama T, Ishiyama T, Ohmura Y. Nikon projection lens update. Proc. SPIE Optical Microlithography 2004; 5377 730.

[4]   Hsu S. H, Fang S. P, Huang I.H, Lin B.S. M, Hung K.C Extension of ArF lithography for poly gate patterning of 65-nm generation and beyond. Proc. SPIE 2004; 5377 1214.

[5]   Bloomstein T.M, Horn M.W, Rothschild M, Kunz R.R, Palmacci S.T, Goodman R.B. Lithography with 157 nm lasers. J. Vac. Sci. Technol. 1997; (B15) 2112.

[6]   Grenville A, Liberman V, Rothschild M, Sedlacek J.H.C, French R.H, Wheland R.C, Zhang X, Gordon J. Behavior of candidate organic pellicle materials under 157-nm laser irradiation, Proc. SPIE 2002; (4691) 1644.

[7]   French R, Wheland R.C, Qiu W, Lemon M.F, Blackman G.S, Zhang E, Gordon J, Liberman V, Grenville A, Kunz R.R, Rothschild M. 157-nm pellicles: polymer design for transparency and lifetime. Proc. SPIE 2002; 4691 576.

[8]   Switkes M, Rothschild M. Resolution enhancement of 157-nm lithography by liquid immersion. Proc. SPIE 2002; 4691 459.

[9]   Owa S, Nagasaka H, Nakano K, Ohmura Y. BCurrent status and future prospect of immersion lithography. Proc. SPIE 2006; 6154 (61) 5408-1.

[10] Sewell H, Mulkens J, McCafferty D, Markoya L, Streefkerk B, Graeupner P. B. The next phase for immersion lithography. Proc. SPIE 2006, 6154 615.

[11] Peng S, French R.H, Qiu W, Wheland R.C, Yang M, Lemon M.F, Crawford M.K. Second generation fluids for 193 nm immersion lithography. Proc. SPIE 2005; 5754 427.

[12] Ehrfeld W, Lehr H. Deep X-ray lithography for the production of three-dimensional microstructures from metals, polymers and ceramics. Radiation Physics and Chemistry 1995; 45, (3) 349–365.

[13] Broers A. N, Hoole A. C. F, Ryan J. M. Electron beam lithography--Resolution limits. Microelectronic Engineering 1996; 32 (131 EOF 142)1-4.

[14] Liu K, Avouris P, Bucchignano J, Martel R, Sun S, Michl J. Simple fabrication scheme for sub-10 nm electrode gaps using electron-beam lithography. Applied Physics Letters 2002; 80 (5) 865-867.

[15] Yu-Tung C, Tsung-Nan L, Yong S C, Jaemock Y, Chi-Jen L, Jun-Yue W, Cheng-Liang W,Chen-Wei C, Tzu-En H, Yeukuang H, Qun S, Gung-Chian Y, Keng S L, Hong-

Ming L, Jung Ho J, Giorgio M. Full-field hard x-ray microscopy below 30 nm: a challenging nanofabrication achievement.Nanotechnology 2008; 19 395302.

[16] Tichenor D. A, Kubiak G, Malinowski M, Stulen R. H, Haney S, Berger K. W, Brownet L. A, Freema R. R, Mansfield W M, Wood R, Tennant D. M, Bjorkholm J.E, MacDowell A. A, Bokor J, Jewell T. E, White D. L, Windt D. L, Waskiewicz W K. Diffraction-limited soft-x-ray projection imaging using a laser plasma source. Optics Letters 1991; 16 (20) 1557.

[17] Bilenberga B, Jacobsena S, Schmidta M.S, Skjoldinga L.H.D, Shib P, Bøggilda P, Tegenfeldtc J.O, Kristensena A. High resolution 100 kV electron beam lithography in SU-8. Microelectronic Engineering 2006; 83 (4–9) 1609–1612.

[18] Miklyaev Yu. V, Meisel D. C, Blanco A, Freymann von G, Busch K, Koch W, Enrich C, Deubel M, Wegener M. Three-dimensional face-centered-cubic photonic crystal templates by laser holography: fabrication, optical characterization, and band-structure calculations APPLIED PHYSICS LETTERS VOLUME 2003; 82 (8).

[19] Liyun Z, Wenbi Z, Bingheng X, Qiming Y, Aibing G "Making a photoresist relief hologram with expection groove depth"Proc. SPIE 2866, International Conference on Holography and Optical Information Processing (ICHOIP '96), 316 1996 doi: 10.1117/12.263101

[20] George Odian. Principles of Polymerization. John Wiley & Sons, Inc 2004 ISBN 0-471-27400-3

[21] Pollino J, Nair K, Stubbs L, Adams J, Weck M "Cross-linked and functionalized 'universal polymer backbones' via simple, rapid, and orthogonal multi-site self-assembly" Tetrahedron 2004 (60) 7205–7215.

[22] Varadan V.K, Jiang X, Varadan VV. Microstereolithography and other fabrication techniques for 3D MEMS. Chichester: Wiley 2001.

[23] Pao Y.H, Rentzepis P.M. LASER-INDUCED PRODUCTION OF FREE RADICALS IN ORGANIC COMPOUNDS. Appl Phys Letters 1965; 6 (5) 93.

[24] Maruo S, Nakamura O, Kawata S.Three-dimensional microfabrication with two-photon-absorbed photopolymerization.Optics Letters 1997; 22 (2) 132-134.

[25] Martineau C, Anemian R, Andraud C, Wang I, Bouriau M, Baldeck P.L. Efficient initiators for two-photon induced polymerization in the visible range. Chem. Phys. Letters 2002; 362 (3-4) 291–295.

[26] Belfield K.D, Schafer K.J, Liu Y.U, Liu J, Ren X.B, Van Stryland E.W. Multiphoton-absorbing organic materials for microfabrication, emerging optical applications and non-destructive three-dimensional imaging. J. Phys. Org. Chem 2000; 13 (12) 837–849.

[27] Yu-fang Z, Sheng-yu F, Xiao-mei W. Investigation of TPP up-conversion lasing of stilbene derivatives. Journal of Molecular Structure 2002; 613 (1–3) 91–94.

[28] Ajami A, Husinsky W, Liska R, Pucher N. Two-photon absorption cross section measurements of various two-photon initiators for ultrashort laser radiation applying the Z-scan technique. Journal of the Optical Society of America B 2010; 27(11) 2290.

[29] Kumpfmu°ller J, Pucher N, Stampfl J, Liska R. Optical Application in Polymer Photochemistry. New York:Springer Publishers; 2011.

[30] Clay G. O, Schaffer C. B, Kleinfeld D. Large two-photon absorptivity of hemoglobin in the infrared range of 780–880 nm. J. Chem. Physics 2007; 126, (2) 025102.

[31] Tanaka T, Sun HB, Kawata S. Rapid sub-diffraction-limit laser micro/nanoprocessing in a threshold material system. Appl Phys Letters 2002; 80 (2) 312.

[32] Martínez-Corral M, Ibáñez-López C, Saavedra G. Axial gain resolution in optical sectioning fluorescence microscopy by shaded-ring filters. Optics Express 2003; 11 (15) 1740-1745.

[33] Martinez C. M, Pons A. Axial apodization in 4Pi-confocal microscopy by annular binary filters. J. Opt. Soc. Am. A 2002; 19 (8) 1782-1789.

[34] Akturk S, Gu X, Kimmel M, Trebino R. Extremely simple single-prism ultrashort-pulse compressor. OPTICS EXPRESS 2006; 14 (21) 10101-10108.

[35] Teha W. H, Dürig U, Drechsler U, Smith C. G, Güntherodt H. J. Effect of low numerical-aperture femtosecond two-photon absorption on SU-8 resist for ultrahigh-aspect-ratio microstereolithography. Journal of Applied Physics 2005; 97 (5) 054907.

[36] Chung C K, Hong Y Z. Surface modification of SU8 photoresist for shrinkage improvement in a monolithic MEMS microstructure. J. Micromech. Microeng. 2007; 17 207–212.

[37] McHugh M.A, Krukonis V.J. Supercritical Fluid Extraction. Butterworth-Heinemann, Boston, 2nd ed., 1994.

[38] Jipa F, Zamfirescu M, Luculescu C, Dabu R. High-aspect-ratio structures produced by two-photon photopolimerization. J Optoelectron. Adv. Materials 2010;12 (1) 124-128.

[39] Tabak M, Hinkel D, Atzeni S, Campbell E. M, Tanaka K. Fast Ignition: Overview and Background. Fusion Science and Technology 2006; 49 (3) 254-277.

[40] Quéré F, Thaury C, Monot P, Dobosz S, Martin Ph, Geindre J.-P, Audebert P. Coherent Wake Emission of High-Order Harmonics from Overdense Plasmas. Phys. Rev. Lett. 2006; 96 (12) 125004.

[41] Tahir N. A, D. Hoffmann H. H, Kozyreva A, Shutov A, Maruhn J. A, Neuner U, Tauschwitz A, Spiller P, Bock R. Shock compression of condensed matter using intense beams of energetic heavy ions. Phys. Rev. E 2000; 61 1975–1980.

[42] Fuchs J, Audebert P, Borghesi M, Pepin H, Willi O. Laser acceleration of low emittance, high energy ions and applications. C. R. Physique 2009; 10 176.

[43] Dewald E.L, Suter L.J, Thomas C, Hunter S, Meeker D, Meezan N, Glenzer S.H Bond E, Kline J, Dixit S, Kauffman R.L, Kilkenny J, Landen O.L. First hot electron measurements in near-ignition scale hohlraums on the National Ignition Facility. Journal of Physics: Conference Series 2010; 244 022074.

[44] Galloudec N. R, D'Humieres E. New micro-cones targets can efficiently produce higher energy and lower divergence particle beams. Laser and Particle Beams 2010; 28 513–519.

[45] Buffechoux S, Psikal J, Nakatsutsumi M, Romagnani L, Andreev A, Zeil K, Amin M, Antici P, Burris-Mog T, Compant-La-Fontaine A, d'Humie`res E, Fourmaux S, Gaillard S, Gobet F, Hannachi F, Kraft S, Mancic A, Plaisir C, Sarri G, Tarisien M, Toncian T, Schramm U, Tampo M, Audebert P, Willi O, Cowan T. E, Pe´pin H, Tikhonchuk V, Borghesi M, Fuchs J. Hot Electrons Transverse Refluxing in Ultraintense Laser-Solid Interactions 2010; PHYSICAL REVIEW LETTERS 105 015005.

[46] Ceccotti T, Le´vy A, Popescu H, Re´au F, D'Oliveira P, Monot P, J. Geindre P, Lefebvre E, Martin Ph. Proton Acceleration with High-Intensity Ultrahigh-Contrast Laser Pulses. PHYSICAL REVIEW LETTERSPRL 2007; 99 185002.

[47] Schmid H, Biebuyck H, Michel B, Martin O. J. F. Light-coupling masks for lensless, subwavelength optical lithography. Appl. Phys. Lett.:1998 72 (19) 2379-2381.

[48] Borchers B, Bekesi J, Simon P, Ihlemanna J. Submicron surface patterning by laser ablation with short UV pulses using a proximity phase mask setup. JOURNAL OF APPLIED PHYSICS 2010; 107 063106

[49] Popescu M. Non-Crystalline Chalcogenides. Dordrecht: Kluwer Academic Publishers; 2000.

[50] Jain H., Vlcek M. Glasses for lithography. Journal of Non-Crystalline Solids 2008; 354 1401-1406.

[51] Kovalskiy A., Cech J, Vlcek M., Waits CM, Dubey M., Heffner WR, Jain H. Chalcogenide glass e-beam and photoresists for ultrathin grayscale patterning. J. Micro/Nanolith. MEMS MOEMS 2009; 8(4) 043012.

[52] Popescu M., Disordered chalcogenide optoelectronic materials: Phenomena and applications J. Optoelectron. Adv. Mater. 2005; 7(4) 2189-2210.

[53] De Neufville JP, Moss SC, Ovshinsky SR. Photostructural transformations in amorphous As2Se3 and As_2S_3 films. J. Non-Cryst. Solids 1974; 13(2) 191-223.

[54] Tanaka K. Reversible photostructural change: Mechanisms, properties and applications. J. Non-Cryst. Solids 1980; 35-36 1023-1034.

[55] K. Tanaka, A. Odajima, Photodarkening in amorphous selenium. Solid State Commun. 1982; 43(12) 961–964.

[56] Katayama Y., Yao M., Ajiro Y., Inui M., Endo H. Photo-Induced Phenomena in Isolated Selenium Chains. J. Phys. Soc. Jpn. 1989; 58 1811-1822.

[57] Tanaka K., Ohtsuka Y. Transient characteristics of photochromic processes. J. Opt. 1977; 8 121.

[58] Averyanov VL, Kolobov AV, Kolomiets BT, V. Lyubin M. Thermal and optical bleaching in darkened films of chalcogenide vitreous semiconductors. Phys. Status Solidi (a) 1980; (a) 57 81-88.

[59] Hamanaka H., Tanaka K., Matsuda A., Iizima S. Reversible photo-induced volume changes in evaporated As_2S_3 and As4Se5Ge1 films. Solid State Commun. 1976; 19 499-501.

[60] Vateva E., Arsova D., Skordeva E., Pamukchieva V. Irreversible and reversible changes in band gap and volume of chalcogenide films. J. Non-Cryst. Solids 2003; 326-327 243-247.

[61] Hisakuni H., Tanaka K. Giant photoexpansion in As_2S_3 glass. Appl. Phys. Lett. 1994; 65 2925-2927.

[62] Tanaka K. Spectral dependence of photoexpansion in As_2S_3 glass. Phil. Mag. Lett. 1999; 79 25-30.

[63] Ramachandran S., Pepper JC, Brady DJ, Bishop SG, Micro-optical lenslets by photoexpansion in chalcogenide glasses. J. of Lightwave Technol. 1997; 15 1371-1377.

[64] Saliminia A., Galstian TV, Villeneuve A. Optical Field-Induced Mass Transport in As_2S_3 Chalcogenide Glasses. Phys. Rev. Lett. 2000; 85, 4112-4115.

[65] Tanaka K., Saitoh A., Terakado N. Giant photo-expansion in chalcogenide glass. J. Optoelectron. Adv. Mater. 2006 2058-2065.

[66] Saitoh A., Gotoh T., Tanaka K. Chalcogenide-glass microlenses for optical fibers. J. Non-Cryst. Solids 2002; 299-302 983-987.

[67] Saitoh A., Tanaka K. Self-developing aspherical chalcogenide-glass microlenses for semiconductor lasers. Appl. Phys. Lett. 2003; 83 1725-1727.

[68] Messaddeq SH, Siu Liu M., Lezal D., Ribeiro SJL., Messaddeq Y. Above bandgap induced photoexpansion and photobleaching in Ga–Ge–S based glasses. J. Non-Cryst. Solids 2001; 284 282-287.

[69] Andriesh AM, Buzdugan AI, Dolghier V, Iovu MS. Modeling of chalcogenide glass structures before and after laser illumination, based on mass spectroscopy data. RO-MOPTO '97: Fifth Conference on Optics, SPIE 1998; 3405 258.

[70] Hisakuni H., Tanaka K. Optical Microfabrication of Chalcogenide Glasses. Science 1995; 270, 974-975

[71] Tanaka K. The charged defect exists? J. Optoelectron. Adv. Mater. 2001; 3 189-198.

[72] Tanaka K. Two-photon absorption spectroscopy of As_2S_3 glass. Appl. Phys. Lett 2002; 80(2) 177-179.

[73] Juodkazis S., Kondo T., Misawa H. Photo-structuring of As_2S_3 glass by femtosecond irradiation. Optics Express 2006; 14(17) 7751-7756.

[74] Velea A., Popescu M., Sava F., Lőrinczi A., Simandan ID, Socol G, Mihailescu IN, Stefan N., Jipa F., Zamfirescu M., Kiss A., Braic V.Photoexpansion and nano-lenslet formation in amorphous As2S3 thin films by 800 nm femtosecond laser irradiation. J. Appl. Phys. 2012; 112 033105.

[75] Zaidi SH, Chu AS, Brueck SRJ. Optical properties of nanoscale, one-dimensional silicon grating structures. J.Appl. Phys. 1996; 80 6997-7000.

[76] Yu Z., Chen L., Wu W., Ge H., Chou SY. J. Vac. Sci. Technol. B 2003; 21 2089-2092.

[77] Popov E., Hoose J., Frankel B., Keast C., Fritze M., Fan TY, Yost D., Rabe S. Low polarization dependent diffraction grating for wavelength demultimlexing. Optics Express 2004; 12 269-275.

[78] Hoose J., Frankel R., Popov E., Neviere M., US Patent 2005: 6,958,859 B2.

[79] Geppert T., Schweizer SL, Gosele U, Wehrspohn RB. Deep trench etching in macroporous silicon. Appl. Phys. A-Mater 2006; 84 237-242.

[80] Gish DA, Summers MA, Brett MJ. Morphology of periodic nanostructures for photonic crystals grown by glancing angle deposition. Photonics Nanostruct. 2006; 4 23-27.

[81] Indutnyy I. Z., Popescu M., Lőrinczi A., Sava F., Min'ko VI, Shepeliavyi PE. Fabrication of submicrometer periodic structures using interference lithography and two-layer chalcogenide photoresist. J. Optoelectron. Adv. Mater. 2008; 10(12) 3188 – 3192.

[82] [82 Popescu A., Savastru D., Miclos S. Refractive index anisotropy in non-crystalline As_2S_3 films. J. Optoelectron. Adv. Mater. 2010; 12 (5) 1012-1018

[83] Bayindir M., B. Temelkuran, Ozbay E. Tight-Binding Description of the Coupled Defect Modes in Three-Dimensional Photonic Crystals. Phys. Rev. Lett. 2000; 84 2140-2143

[84] Noda S., Tomoda K., Yamamatu N., Chutinan A. Full Three-Dimensional Photonic Bandgap Crystals at Near-Infrared Wavelengths. Science 2000; 289 604-606

[85]   Popescu A., Micloş S., Savastru D., Savastru R., Ciobanu M., Popescu M., Lőrinczi A., Sava F., Velea A., Jipa F., Zamfirescu M. Direct laser writing of two-dimensional photonic structures in amorphous As_2S_3 thin films. J. Optoelectron. Adv. Mater. 2009; 11(11) 1874-1880.

[86]   Popescu M., Sava F., Lőrinczi A., Velea A., Vlček M., Jain H. Modelling of dissolution kinetics of thin amorphous chalcogenide films. Phil. Mag. Lett. 2009; 89(6) 370-376.

[87]   Popescu M., Velea A., Lőrinczi A., Zamfirescu M., Jipa F., Micloş S., Popescu A., Ciobanu M., Savastru D. Two-dimensional photonic structures based on As-S chalcogenide glass. Dig. J. Nanomater. Bios. 2010; 5(4) 1101-1105.